Geohazard Mechanics 4 (2026) 44–54

Contents lists available at ScienceDirect

Geohazard Mechanics

journal homepage: www.keaipublishing.com/en/journals/geohazard-mechanics

Application of convolutional neural networks for rock stability identification and failure time prediction

Weiyang Li, Yongxing Shen*, Zengchao Feng**, Xuchen Guo

Key Laboratory of In-situ Property-Improving Mining of Ministry of Education, Taiyuan University of Technology, Taiyuan, 030024, China

ARTICLE INFO

Keywords:
Rock failure time
Convolution model
Precursor of rock failure
Displacement coordination coefficient

ABSTRACT

The identification of rock stability and the prediction of failure time are crucial for the early warning and prevention of sudden geological disasters such as landslides and collapses. To address these challenges, this study proposes three convolutional prediction models: CNN-LSTM-Attention, CNN-BiLSTM-Attention, and CNN-GRU-Attention. The displacement coordination coefficient (DCC) index and stress curves were employed as input variables to evaluate the performance of each model in discriminating rock stability states under different data structures and input configurations. Furthermore, an innovative methodology for predicting rock failure time utilizing convolutional models was developed. The experimental results demonstrate that the CNN-LSTM-Attention model, utilizing a 10 × 10 × 2 data structure, exhibits superior performance in rock stability state discrimination, achieving an accuracy of 95.25 % on the validation set and a recall rate of 96 % for samples in high-risk areas. Furthermore, when the DCC index was used as the input variable, the CNN-LSTM-Attention model achieved recall rates of 95.8 % and 86.5 % for medium- and high-risk areas, respectively, in the validation set. These findings indicate that the proposed convolutional models can effectively identify rock stability states by leveraging surface deformation characteristics. The CNN-LSTM-Attention model, with the DCC index as the input variable, is capable of predicting the final rock failure time in real-time once the DCC abrupt change exceeds 0.78. For different rocks, the model can predict the failure time within 20 s after the DCC reaches 0.78, with an error rate of less than 9 %. The convolutional neural network model, developed based on the DCC index, provides a novel methodological approach for geohazard early warning research, facilitating slope instability monitoring and earthquake precursor identification using GNSS and other displacement measurement techniques.

1. Introduction

The prediction of geological disasters such as earthquakes, landslides, and collapses is a key research area [1]. In the active area of strong earthquakes, rock mass instability often causes chain collapse disasters, while the sudden damage of rainfall landslides poses a serious threat to mountain residents. Accurate prediction of such events in rock mass systems is of great significance for disaster prevention and mitigation [2]. Rock failure prediction serves as a fundamental scientific model, simplified from these major applications and associated scientific challenges [3]. However, the inherent heterogeneity and anisotropy of rocks introduce uncertainty and sample-specific variability into the failure and instability processes. Consequently, even samples with similar initial states may exhibit markedly divergent nonlinear evolution characteristics as they approach failure [4,5]. Due to the complexity of capturing these nonlinear evolution dynamics, it is imperative to identify precursor indicators of rock failure and develop predictive models for early warning systems. The model is crucial for accurately identifying rock stability and reliably predicting rock failure time, and may be further applied to the prediction of geological disasters.

Extensive research has been conducted by scholars worldwide on the precursor information of rock failure, with particular emphasis on the deformation field characteristics of rock surfaces. Pan et al. [6] proposed a rock burst prediction method utilizing the localization of coal and rock deformation as a precursor, grounded in the energy principles of classical mechanics, based on the intrinsic properties of coal and rock

* Corresponding author.
** Corresponding author.
E-mail addresses: syx754578945@163.com (Y. Shen), zc-feng@163.com (Z. Feng).
Peer review under the responsibility of Liaoning University.

https://doi.org/10.1016/j.ghm.2026.01.002
Received 26 February 2025; Received in revised form 19 August 2025; Accepted 5 January 2026
Available online 6 January 2026

deformation and the underlying mechanisms of rock burst instability. Wang et al. [7] analyzed deformation fields at various stages of multiple uniaxial compression tests to identify the mechanical factors governing the localization area's position and growth direction. They further investigated monitoring and early warning indicators based on deformation localization, integrating these findings with axial force-displacement relationship curves. Wang et al. [8] conducted uniaxial compression tests on rectangular coal samples, comparing the deformation processes of horizontal line strain, shear strain, maximum shear strain, and volumetric strain. They characterized the onset of strain localization using abrupt changes in the coefficient of variation, thereby facilitating the identification of failure precursors in coal samples. In laboratory-based rock mechanics experiments, Shen and Feng [9] monitored the complete failure process of rocks under uniaxial compression and introduced a method for predicting peak rock strength using the coefficient of variation of multi-point displacement increments on the rock surface. This method demonstrated a sharp increase in the coefficient of variation of displacement increments prior to peak stress, providing a reliable precursor for rock failure instability. Cheng [10] conducted failure tests on intact and prefabricated fractured rock samples, proposing an inhomogeneous deformation index as a precursor for rock deformation instability; and the study revealed a significant correlation between the stage-wise characteristics of the inhomogeneous deformation index and the evolutionary states of rock damage. Furthermore, Shen et al. [11] introduced the displacement coordination coefficient (DCC) index based on displacement field data from finite measuring points on rock surfaces, investigated the evolution characteristics of DCC during the failure processes of different rocks, and quantitatively analyzed the temporal sensitivity of DCC to rock instability. Through mathematical statistics, they established a quantitative threshold for predicting the occurrence of rock failure instability events.

At the same time, a large number of researchers use neural network model to deal with the problems related to rock destruction. Convolutional neural network (CNN) uses its feature extraction ability. It can effectively analyze the data of information enhancement stability prediction and apply it to the prediction of landslide disaster [12–14]. Fan et al. [15] predicted the temporal and spatial distribution of seismic risk based on CNN-LSTM (long short term memory) and quantitatively evaluated the seismic risk. Li et al. [16] proposed a rockburst prediction method based on microseismic sensitive characteristic index and enhanced convolutional neural network (CNN-GRU(Gated Recurrent Unit), a combined model of convolutional neural network and cyclic recursive unit). Zhao et al. [17] applied squeeze and exception (SE) attention mechanism and DenseNet + GC + SE to predict the remaining time of coal sample failure. Zhanget al. [18] used CNN-LSTM-Attention to realize the time series prediction of tunnel surrounding rock deformation. Combined with the advantages and applications of each model, this paper combines different module combinations as CNN-LSTM-Attention, CNN-Bilstm-Attention, and CNN-GRU Attention to deal with the sensitivity of the precursor index DCC in rock failure time. In addition, neural network models are widely used in other fields. In terms of time series prediction, Li et al. [19–22] have successively proved that CNN-LSTM-Attention and other models in different fields have higher prediction effect than traditional models.

Therefore, based on the excellent performance of CNN-LSTM-Attention, CNN-Bilstm-Attention, and CNN-GRU Attention convolution models in prediction effect, they are applied to the sensitivity processing of DCC to rock failure time. Taking the DCC index and stress curve as input variables, the rock state identification effect of different data structures under each convolution model is studied, and the influence of different input variables on the model identification effect is analyzed. Furthermore, the prediction method of rock failure time based on convolution model is proposed, which provides a novel methodological approach for geohazard early warning research, facilitating slope instability monitoring and earthquake precursor identification using GNSS and other displacement measurement techniques.

2. Rock failure precursor-displacement coordination coefficient (DCC)

2.1. Acquisition of DCC

The DCC serves as an effective indicator for capturing precursor signals of rock instability, with its anomalous surge representing a critical precursor characteristic. Utilizing surface deformation data, DCC facilitates real-time quantitative detection and identification of instability precursors in different rocks prior to failure [11]. The methodology for obtaining DCC values is detailed in study by Qiu et al. [23], while a brief description of its derivation is provided herein.

The experiments were conducted using a servo-controlled testing machine with a maximum load capacity of 3000 kN. During testing, industrial cameras were employed for real-time image acquisition of specimen surfaces, with an image resolution of 4096 × 3000 pixels at a sampling rate of 1 Hz. Speckle patterns were applied to specimen surfaces prior to displacement-controlled uniaxial compression tests. The specimens were loaded at a constant rate of 0.001 mm/s until complete failure, while simultaneously recording stress-strain curves and surface deformation images [23]. Fig. 1 illustrates the schematic diagram and physical photograph of the experimental system.

As shown in Fig. 2, thirty monitoring points were randomly distributed across the rock surface to track displacement variations from initial loading to instability (the curves labeled n1, n2 … n30 in Fig. 3 represent displacement evolution at each monitoring point). Subsequently, the DCC was calculated using Eqs. (1)–(3).

$$\begin{cases} \dfrac{1}{n}\sum_{i=1}^{n} k_i x_i = \dfrac{1}{n}\sum_{i=1}^{n} x_i = \overline{x} \\ a_0\overline{x} = \sqrt{\dfrac{1}{n}\sum_{i=1}^{n}\left(k_i x_i - \overline{x}\right)^2} \end{cases} \tag{1}$$

$$S_i' = \sqrt{\frac{1}{n-1}\sum_{j=1}^{n}\left(x_{ij}' - \overline{x_i'}\right)^2} \tag{2}$$

$$DCC_i = \frac{S_i'}{\overline{x_i'}} \tag{3}$$

where S_i' is the standard deviation of normalized absolute displacements across all monitoring points at time i; $\overline{x}_i'$ is the mean value of normalized absolute displacements at time i; and DCC_i is the multi-point DCC at time i.

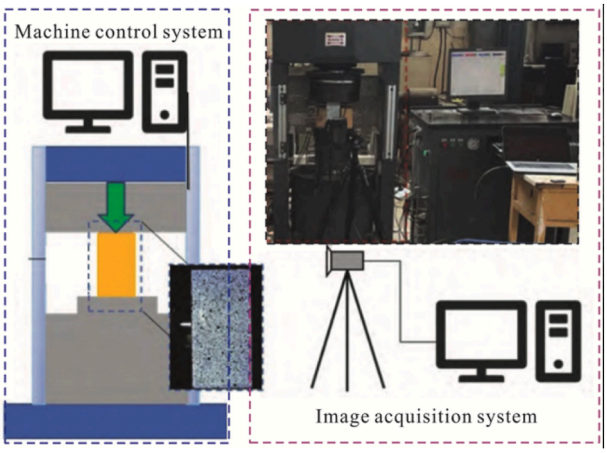

Fig. 1. Schematic diagram of test equipment [11].

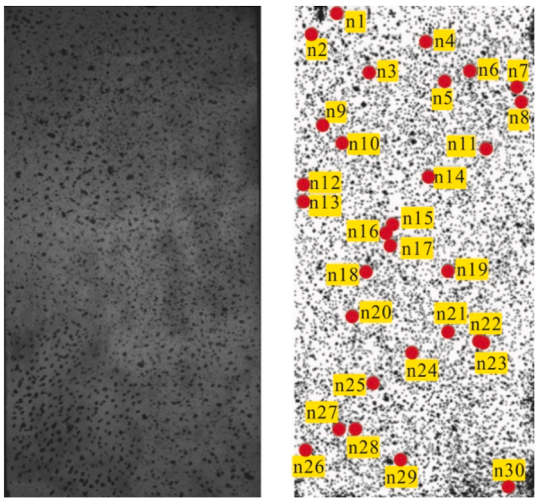

Fig. 2. Diagram of rock surface monitoring points.

2.2. Characteristics of DCC

The variation characteristics of DCC are closely related to the deformation of rock. Fig. 3 shows the displacement deformation rate, DCC, and the relationship between stress and time for various measurement points during marble loading. In the loading time from 0 to 400 s, the displacement increment curves for various measurement points on the rock surface remain flat, indicating a phase of constant deformation speed, which is the linear deformation stage. The deformation coordination among various measurement points is relatively good, and the DCC curve remains stable at a value of approximately 0.1. However, when the loading time approaches 400 s, at which point the axial stress on the rock reaches 68.7 MPa and achieves 90 % of the peak stress, the displacement deformation rate curves for various measurement points start to deviate from the horizontal to varying degrees. Some points show positive growth, while others show negative growth, exhibiting a certain degree of random variation.

There is a deviation in the deformation coordination consistency of each measurement point, and the DCC shows a sudden increase at 410 s, reaching a maximum value of 1.43 at 478 s. At this time, the stress state of the rock is 75.5 MPa, which is 99.0 % of the peak stress. Subsequently, the trends of various measurement points tend to stabilize, and the deformation coordination level of each measurement point begins to recover. At this point, the DCC curve shows a certain degree of decreasing trend. In summary, the DCC index calculated based on the displacement information of various points on the rock surface sensitively and accurately captures the transition from linear to nonlinear deformation before rock failure. The sudden increase in its value is a key precursor feature of rock failure. Moreover, the variation of the DCC index is closely related to the stress state of the rock.

For the deeper change of DCC index, Fig. 4 illustrates the evolution curves of stress, displacement increment, and DCC indices for six samples of marble, yellow sandstone, and purple sandstone during uniaxial compression tests over time. The stress curves exhibit a rapid decline after reaching their peak, followed by rock failure, with the stress trends being largely consistent across different rock types. Similarly, the displacement increment trends are comparable among the rocks, characterized by a sharp initial increase prior to failure, although significant numerical variations are observed. In the uniaxial compression experiments of the six rock samples depicted in Fig. 4, the DCC curves display an abnormal surge preceding rock failure and instability, serving as a precursor to these events [11]. However, the microscopic disorder and heterogeneity inherent in the rock's inhomogeneous medium result in sample-specific macroscopic behaviors, which are also reflected in the sample-specific characteristics of the DCC curves [24–26]. Specifically, in Fig. 4a, the DCC curve for marble1 exhibits an abnormal increase at 408 s, with rock failure occurring at 512 s, resulting in a time interval of 104 s, which accounts for 19.9 % of the total loading time. In Fig. 4b, the DCC curve for marble2 shows an anomalous increase at 638 s, followed by rock failure at 677 s, with a time interval of 39 s (5.7 % of the total loading time). In Fig. 4c, the DCC curve for yellow sandstone1 increases abnormally at 508 s, and rock failure occurs at 701 s, yielding a time interval of 193 s (27.5 % of the total loading time). In Fig. 4e, the DCC curve for purple sandstone1 demonstrates an abnormal increase at 740 s, with rock failure at 826 s, resulting in a time interval of 86 s (10.4 % of the total loading time). These findings indicate that while the abrupt change in the DCC curve is a definitive precursor to rock failure and instability, it does not provide precise prediction of the exact failure time. Consequently, further research and novel methodologies are required to address this limitation.

3. Convolution model for identifying the rock steady state and predicting the failure time

3.1. Convolutional model structure

In recent years, the advancement of neural network research has demonstrated significant efficacy in addressing nonlinear problems. Consequently, this study employs the DCC index as an input for the convolutional model to facilitate the identification of rock failure states and subsequent prediction of rock failure time.

The convolutional models introduced in this study comprise CNN-GRU-Attention, CNN-BiLSTM-Attention, and CNN-LSTM-Attention. As illustrated in Fig. 5, convolutional neural networks (CNN) [27,28] simulate biological neural mechanisms by employing convolutional layers to extract features from the DCC index. Subsequently, the pooling layer reduces the dimensionality of the feature data, enabling the extraction of higher-level effective features with reduced computational

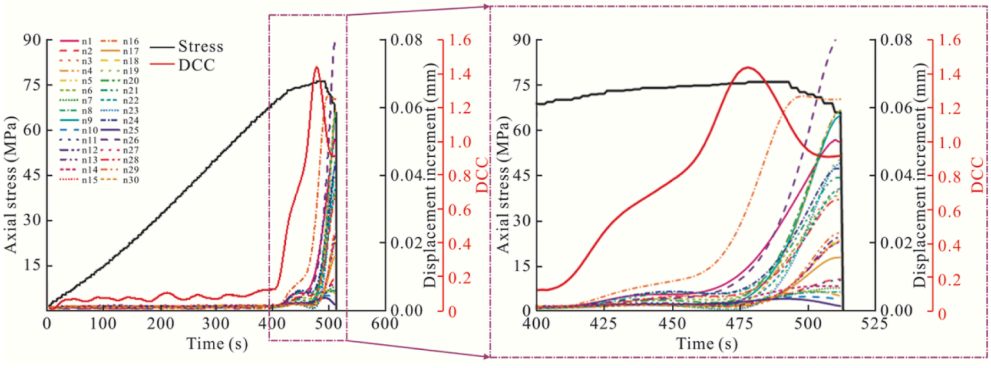

Fig. 3. Displacement deformation rate of the rock surface measurement point, as well as the stress and the evolution of the DCC with loading time.

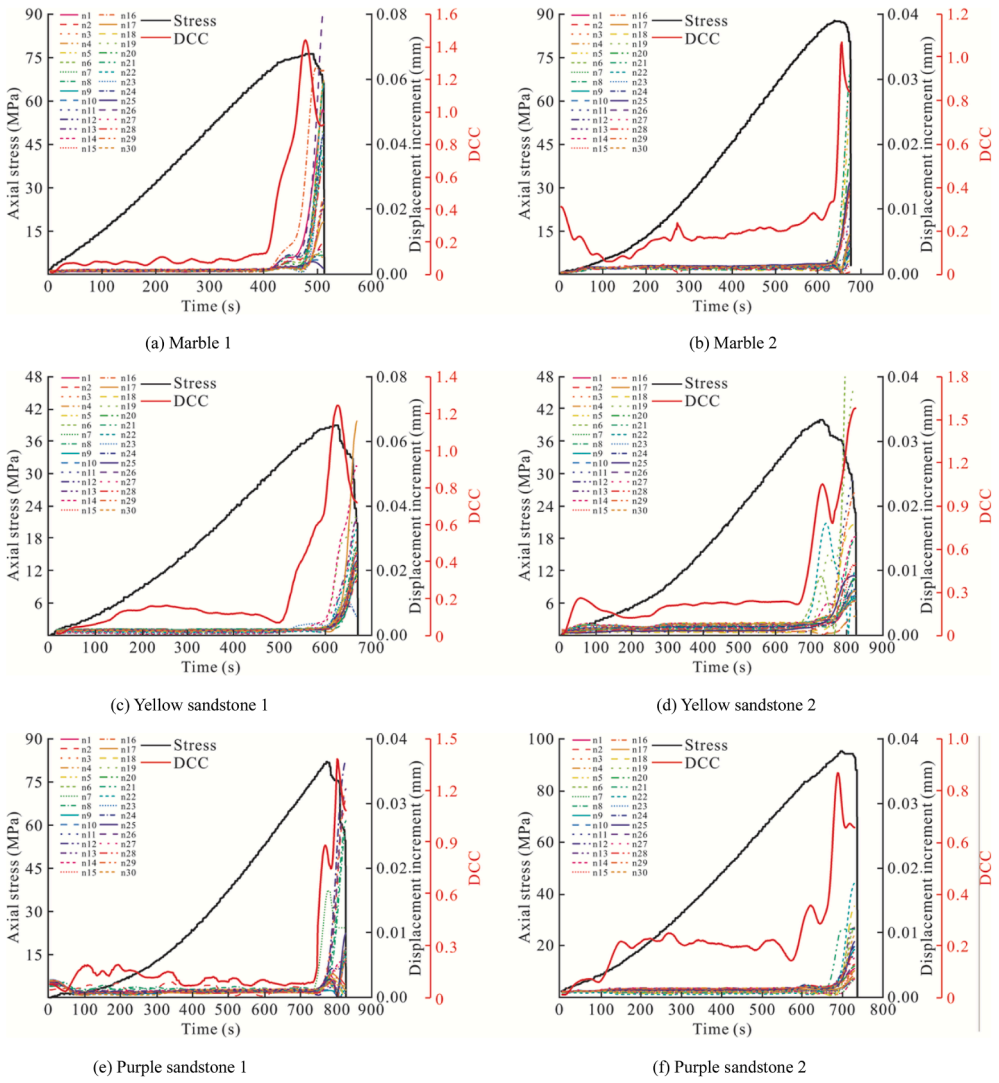

Fig. 4. Temporal evolution curves of uniaxial compressive stress, displacement increment and displacement coordination coefficient of rock.

complexity. The recurrent neural network (RNN) units integrated into these models include the long short-term memory (LSTM) model [29], the Gated Recurrent Unit (GRU) model [30], and the Bidirectional long short-term memory (BiLSTM) model, which combines forward and backward LSTM layers. This architecture allows the convolutional models to selectively retain or discard previous information, thereby facilitating the effective utilization of rock data across the temporal dimension. Furthermore, the Attention mechanism [31] enhances the model's performance by dynamically establishing global correlations among feature data and constructing nonlinear relationships between input parameters and rock failure.

3.2. Data preprocessing

Prior to employing the three convolutional models, the input data must undergo appropriate preprocessing to ensure accurate processing and interpretation by the model. As depicted in Fig. 6, the DCC index and stress curve were utilized as the raw data, with sampling conducted at any arbitrary time point t during the rock loading process. Based on the DCC evolution curve, which exhibits an abrupt change upon reaching a threshold of 0.78 [11] when the loading time accounts for approximately 85 % of the total duration, the rock failure risk level was categorized according to the time proportion, as outlined in Table 1. To streamline the dataset and enhance the model's learning efficiency, the original dataset was constructed by sampling at 10 s intervals in Region I and at 1 s intervals in Regions II, III, and IV. The sampling area was divided into four risk areas based on the remaining time to rock failure at time t, as illustrated in Fig. 6. The risk area corresponding to the area at time t serves as the output of the convolutional model. The input sequence of the convolutional model can be interpreted as a "response" of the rock at time t [17], describing its state at that moment. This sequence encapsulates all historical information, forming a Markov chain [32], which facilitates the generalization of the model.

Furthermore, to enhance the predictive performance of the convolutional model and optimize the utilization of rock information across the temporal dimension, this study employs two distinct data structures to standardize data with varying time steps, thereby ensuring consistency in the input data. The impact of these data structures on the accuracy of the convolutional model is subsequently evaluated. The DCC and stress curve sampled in Fig. 6 are uniformly processed into a three-dimensional matrix with dimensions of either $1000 \times 2 \times 1$ or $10 \times 10 \times 2$.

As illustrated in Fig. 7, two data structures are generated through data processing. The first data structure is based on the consideration of data time order, which interpolates and extends the original data to 1000 time steps, converts the time series data into the corresponding three-dimensional matrix, and further converts it into gray image. The second data structure is for the reason of CNN calculation. Convolutional

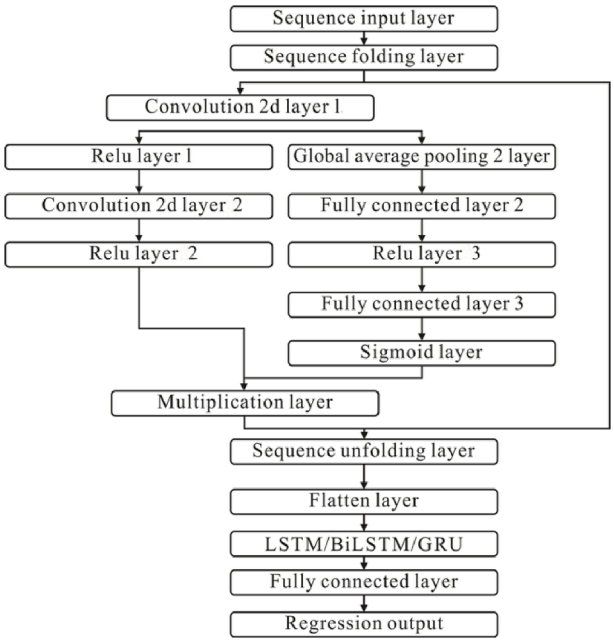

Fig. 5. Convolutional model structure.

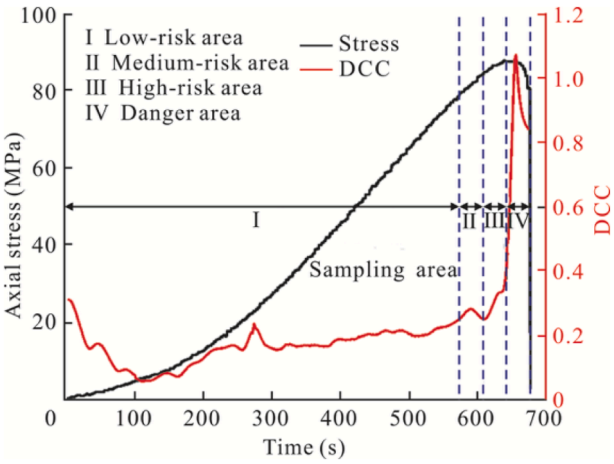

Fig. 6. Risk area segmentation of rock.

Table 1
Classification of rock failure risk levels and number of sample.

Rock damage risk level	Time percentage (%)	Number of sample
Low-risk area	0–85	790
Medium-risk area	85–90	1000
High-risk area	90–95	990
Danger area	95–100	1020

neural network (CNN) has the characteristics of local perception, weight sharing and pool operation, and shows good feature extraction ability in image recognition. The time series data are reconstructed into a 10 × 10 × 2 three-dimensional tensor structure, whose dimensions correspond to time step, characteristic channel and signal segmentation, respectively. The original data is compressed into 100 time steps, the data with 100 time steps is converted into 10 × 10 sequence data, and then it is converted into gray image.

In order to construct a comprehensive data set, 50 rock samples (ten granite, yellow sandstone, purple sandstone, marble and basalt) were sampled for DCC and stress curve, and 3800 corresponding data sets were generated. Table 1 presents the sample distribution of each risk area. In these data sets, 70 % data sets were used for model training, and the remaining 30 % data sets were used for model validation.

3.3. Data annotation and training parameter selection

For each sample input into the convolutional model, the remaining time until rock failure is defined as $d\_t{:}T_{max}\text{-}t$. Based on the framework illustrated in Fig. 6, the rock failure risk level was categorized, with each sample assigned a risk level according to the criteria outlined in Table 1 [17]. The CNN-LSTM-Attention, CNN-BiLSTM-Attention, and CNN-GRU-Attention convolutional models were implemented using Matlab software to identify the rock failure risk level. The predictive performance of these three convolutional models was subsequently compared. Training was conducted using Intel's i7-8565U processor, with unified training parameters applied across all models, as detailed in Table 2.

3.4. Model evaluation metrics

To evaluate the performance of the prediction model, the following evaluation indicators are introduced.

(1) Model complexity: The complexity of the model reflects the number of parameters contained in the model (MB). The more parameters, the more complex the model.
(2) Time complexity: The time complexity indicates the time (s) required to train a convolutional model, and the longer it takes, the lower the model efficiency.
(3) Accuracy: The accuracy reflects the model's ability to predict the sample. Taking the accuracy of low-risk areas as an example, it can be explained by how many of the samples predicted as low-risk areas are really low-risk areas. It is calculated as follows [33]:

$$Accuracy = \frac{\sum_L^N sign(Y_L = \widehat{Y_L})}{N} \tag{4}$$

where *sign* is the sign function, and if $Y_L = \widehat{Y_L}$, that is, when the sample prediction label is consistent with the real label of the sample, the sign function returns 1, otherwise it returns 0.

(4) Recall: Recall reflects the model's ability to capture samples. Taking the recall rate of low-risk areas as an example, it can be explained by how many low-risk areas are predicted in the real low-risk area sample. It is calculated as follows [33]:

$$Recall = \frac{\sum_L^S sign(Y_L = \widehat{Y_L})}{S} \tag{5}$$

where S is the total number of samples in the corresponding risk area, and the closer the recall rate is to 1, the better it is.

(5) Micro-F1: Micro-F1 is used to measure the overall performance of the model when the categories are unbalanced or focus on a few classes. It is calculated as follows:

$$Micro - F1 = 2^* \frac{Accuracy^* Recall_{total}}{Accuracy + Recall_{total}} \tag{6}$$

where $Recall_{total}$ is the regression rate of all samples and all categories, which is different from the recall in Eq. (5) to show the difference.

4. Rock steady state discrimination effect

In Section 3, the CNN-LSTM-Attention, CNN-BiLSTM-Attention, and CNN-GRU-Attention convolutional models were trained using both 1000 × 2 × 1 and 10 × 10 × 2 data structures. In this section, a

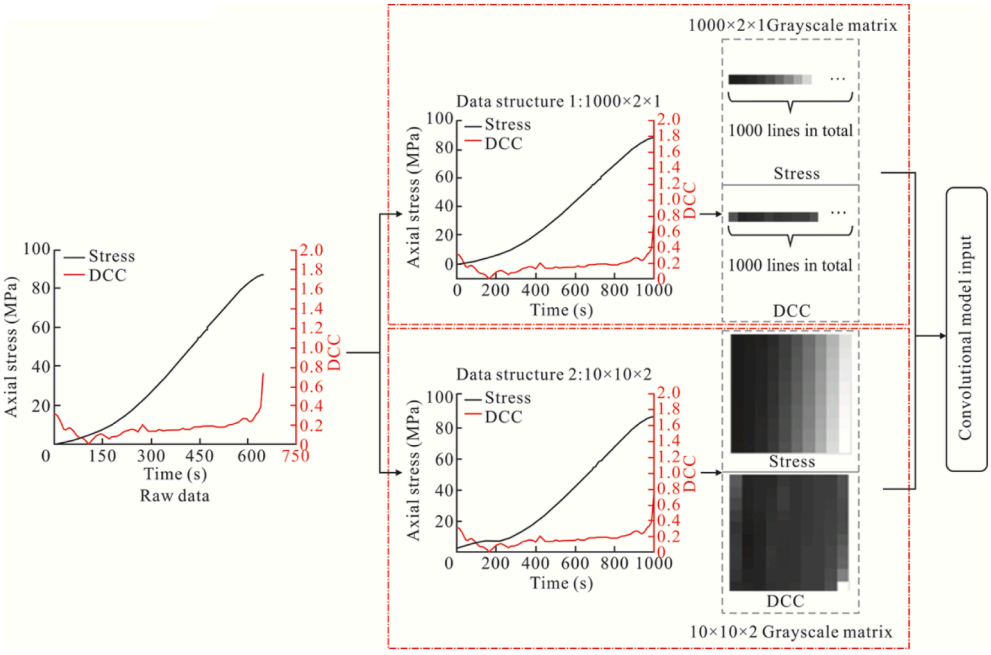

Fig. 7. Data normalization methods.

Table 2
Convolutional model parameters.

Convolutional model parameter	Parameter
Initial learning rate	0.001
Maximum number of training epochs	1000
Learning rate decline factor	0.1
Regularization parameters	0.0001
Learning rate decline cycle	100
Activate the function	Relu
Gradient descent algorithm	Adam

comprehensive analysis is conducted to evaluate the effectiveness of these convolutional models in discriminating rock stability states across different data structures, as well as their performance under varying input variables.

4.1. Rock steady state discrimination effect of different data structures in different convolution models

As shown in Table 3, the 1000 × 2 × 1 data structure is used to distinguish the rock stability of the three convolution models. The accuracy of the validation set is 68.75 % at least and 81.25 % at most. The recall rate of samples in high-risk areas remains below 80 %. In contrast, the performance of the 10 × 10 × 2 data structure has been significantly improved, the accuracy of the validation set is more than 91.25 %, and the maximum is 95.25 %. In addition, the sample recall rate in high-risk areas has always exceeded 95 %. The Micro-F1 (91.7–94.1 %) and AUC (0.92–0.96) of the 10 × 10 × 2 structure are far more than those of the 1000 × 2 structure (Micro-F1:71.1–76.2 %, AUC:0.78–0.84), indicating that the data dimension reorganization greatly improves the performance of the model.

Compared to the convolutional model trained using the 1000 × 2 data structure, the 10 × 10 × 2 data structure exhibits a reduced number of parameters and lower time complexity. The results demonstrate that the input data structure of the convolutional model significantly enhances model accuracy, effectively reduces computational load, improves model efficiency, and facilitates deployment in real-world rock failure monitoring applications. Among the three convolutional models evaluated under the 10 × 10 × 2 data structure, the CNN-LSTM-Attention model achieved the highest performance, the accuracy of the validation set for high-risk samples was 95.25 %, the recall rate was 96 %, the micro-F1 was 94.4 %, and the AUC was 0.96.

In summary, the 10 × 10 × 2 data structure demonstrates superior performance compared to the 1000 × 2 × 1 data structure, and the CNN-LSTM-Attention model outperforms the CNN-BiLSTM-Attention and CNN-GRU-Attention models. Specifically, the CNN-LSTM-Attention model under the 10 × 10 × 2 data structure emerges as the optimal model, achieving a rock stability state discrimination accuracy of 95.25 % on the validation set and a recall rate of 96 % for high-risk samples.

4.2. Rock steady state discrimination effect of convolution model under different input variables

To quantitatively analyze the critical role of the DCC in the

Table 3
Discriminative effect of convolutional model on rock stability state.

Data structure	Convolutional model structure	Number of parameters (MB)	Time complexity (s)	Validation set			
				Accuracy (%)	Danger area recall (%)	Micro-F1 (%)	AUC
1000 × 2	CNN-LSTM-Attention	30	19971	81.25	72.00	75.40	0.84
	CNN-BiLSTM-Attention	61	24623	78.75	73.37	76.20	0.82
	CNN-GRU-Attention	23	20277	68.75	76.67	71.10	0.78
10 × 10 × 2	CNN-LSTM-Attention	1.27	2995	95.25	96.00	94.40	0.96
	CNN-BiLSTM-Attention	2.54	4079	95.00	95.50	93.20	0.95
	CNN-GRU-Attention	0.96	2671	91.25	94.00	91.70	0.92

convolutional model and enhance the model's interpretability, this study leverages the optimal data structure and convolutional model identified in the preceding section: the CNN-LSTM-Attention model under the $10 \times 10 \times 2$ data structure. Three distinct input variable configurations (stress, displacement coordination coefficient, and stress combined with displacement coordination coefficient) were employed to train the aforementioned convolutional model. The influence of these input variables on the model's recognition performance was systematically compared and analyzed.

The rock stability state discrimination results for different input variables in the training set and validation set are presented in Figs. 8 and 9. The accuracy of rock stability state discrimination, ranked from low to high for both the training and validation sets, is as follows: stress, DCC, and stress combined with displacement coordination coefficient. Specifically, the training set accuracies are 63.33 %, 88.66 %, and 95 %, while the validation set accuracies are 51.25 %, 78.75 %, and 90 %. These results indicate that the accuracy of rock stability state discrimination is significantly influenced by the input variables of the convolutional model. Compared to the stress curve, the DCC more effectively captures the evolution process of rock failure instability. This demonstrates that the DCC index, as a dimensionless quantity normalized by considering the initial deformation characteristics of each rock, enables real-time identification of the precursor moment of instability for different rocks. When stress combined with DCC is used as the input variable, the validation set recall rates for low-risk, medium-risk, high-risk, and dangerous areas are 76.5 %, 95.7 %, 94.1 %, and 95.5 %, respectively, with an overall accuracy of 90 %. The convolutional model based on stress combined with DCC achieves an accuracy of 90 % for predicting rock failure time across the four risk areas and 95.5 % for rocks in the dangerous area.

However, in the process of geological disasters, it is a great challenge to directly obtain the internal stress information of rock mass, but the deformation field information of rock surface can be efficiently obtained through modern remote sensing monitoring technology, so as to derive the evolution law of the surface DCC index of rock mass. Consequently, the convolutional model based on the DCC index holds greater engineering value and practical significance for the accurate prediction of rock failure time. As shown in Figs. 8 and 9, the convolutional model utilizing the DCC index as the input variable demonstrates optimal performance in identifying medium-risk areas, achieving an accuracy of 95.8 %. The recall rate for medium-risk areas (95.7 %) is 0.1 % higher than that of the convolutional model using stress combined with DCC as the input variable. Additionally, the recall rate for high-risk areas is 86.5 %, only 7.6 % lower than that of the high-risk areas (94.1 %) under the convolutional model with stress combined with DCC as the input variable. These results indicate that the recall rates for medium-and high-risk areas on the validation set reach 95.8 % and 86.5 %, respectively, when the DCC index is employed as the input variable for the CNN-LSTM-Attention model, effectively enabling the identification of rock stability states.

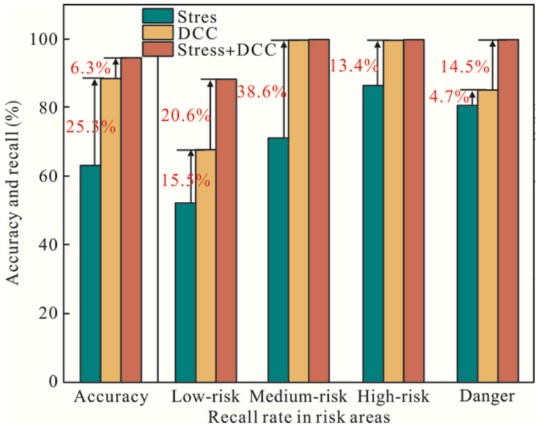

Fig. 8. Training set discrimination effect.

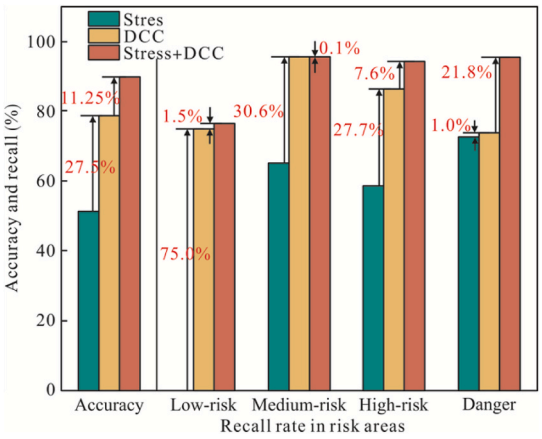

Fig. 9. Verifying the set discrimination effect.

4.3. Ablation test of CNN-LSTM-attention

In Section 4.2, it is proved that taking the DCC index as the input variable of the optimal CNN-LSTM-Attention model can effectively realize the identification of rock stability. Furthermore, ablation tests were conducted to observe the importance of each module in rock stability judgment and verify the improvement of attention mechanism in rock stability judgment.

According to the testing plan of the ablation experiment, four different deep learning model architectures were systematically reorganized, including the CNN model, LSTM model, CNN-LSTM model and CNN-LSTM Attention model with attention mechanism introduced. Using the DCC curve as the unified input variable for the four models mentioned above is to ensure comparability of experimental conditions. Each model is independently trained and validated using the same training and testing sets, and its performance in rock stability recognition tasks is comprehensively evaluated through three key indicators: confusion matrix, recall, and accuracy.

Table 4 and Fig. 10 show the accuracy, recall, and confusion matrices of four models on the validation set. In the comparison of different module combinations, the attention mechanism has improved the performance in all aspects (the accuracy rate has increased by 9.4 %–15.1 %). It has the most significant effect on improving the identification of medium and high risks (the recall rate in the medium risk area has increased by 6.9 %–11.3 %, and the recall rate in the high risk area has increased by 5.6 %–10.8 %). The identification of danger areas has improved significantly (the recall rate has increased by 6.8 %–11.9 %), which is particularly important for the identification of safety critical scenes, and may be further applied to engineering practice.

Table 4
Accuracy and recall of different model validation sets.

Model	Accuracy (%)	Recall (%)			
		Low-risk	Medium-risk	High-risk	Danger
CNN	63.5	56.9	84.5	75.7	67.2
LSTM	65.1	58.4	86.6	77.7	69.3
CNN-LSTM	69.2	62.0	88.9	80.9	72.3
CNN-LSTM-Attention	78.6	67.1	95.8	86.5	79.1

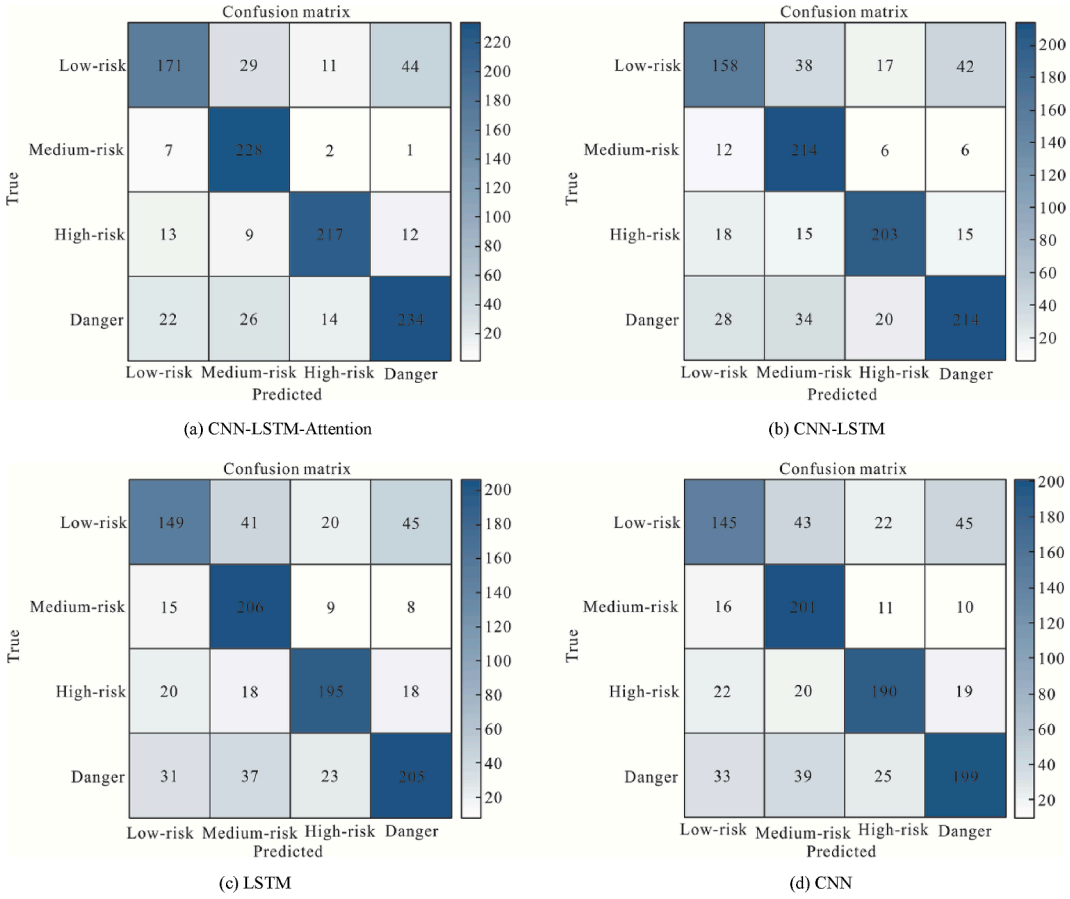

(a) CNN-LSTM-Attention (b) CNN-LSTM

(c) LSTM (d) CNN

Fig. 10. Confusion matrix of different model validation sets.

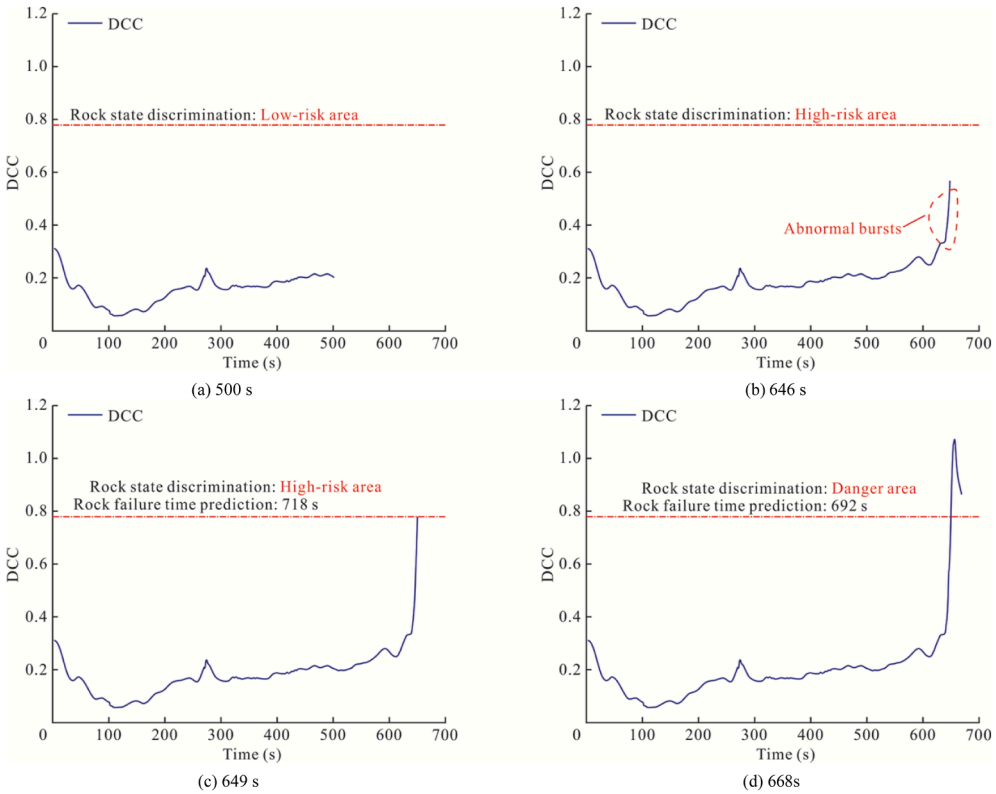

(a) 500 s (b) 646 s

(c) 649 s (d) 668s

Fig. 11. Marble real-time prediction interface.

5. Real-time prediction of rock failure time

Based on the findings presented in Section 4, the CNN-LSTM-Attention convolutional model, combined with the DCC index, can be effectively utilized to identify rock stability states. Feng et al. [34] used the comprehensive experimental statistics to establish the elastoplastic critical threshold for rock deformation transition at 0.98 ± 0.2; and for the small-scale specimens in this paper, the DCC elastoplastic threshold is set to 0.78. The results demonstrate that rock instability initiates when the DCC exceeds this threshold. Building on this foundation, we develop a predictive model for ultimate failure time based on the DCC elastoplastic threshold.

5.1. Real-time prediction process of rock failure time

Using the marble 2 sample with dimension of 50 mm × 50 mm × 100 mm as a representative example, the real-time prediction process of its failure time is outlined as follows:

(1) Obtain the surface deformation field information of marble 2, and calculate the displacement coor-dination coefficient index DCCi in real time;
(2) According to Feng et al. [34], the quantitative threshold of the DCC for the short-term precursor index of rock instability failure is determined to be 0.98 ± 0.2. For small-scale marble specimens with dimension of 50 mm × 50 mm × 100 mm, the abrupt change in DCC, exceeding 0.78, serves as the initiating moment for the convolutional model to predict the failure time of marble.

As illustrated in Fig. 11a, during the real-time prediction process for marble 2, when the DCC evolution curve remains stable at 500 s, the convolutional model classifies marble 2 as being in the low-risk area, and no rock failure time is predicted. In Fig. 11b, the DCC evolution curve exhibits an anomalous increase at 646 s but does not exceed the threshold of 0.78. Consequently, the convolutional model identifies marble 2 as being in the high-risk area, yet no rock failure time is predicted. In contrast, as depicted in Fig. 11c, after the DCC evolution curve undergoes an abrupt surge and surpasses 0.78 at 649 s, the convolutional model classifies marble 2 as being in the high-risk area and predicts its failure time to be 718 s (the actual failure time was 676 s).

(3) As depicted in Fig. 11d, the real-time prediction result generated by the convolutional model at 668 s indicates that marble 2 is located within the danger area, with a predicted rock failure time of 692 s, which deviates from the actual failure time by 16 s. When the DCC evolution curve of the rock exhibits an abrupt surge and exceeds the threshold of 0.78, the convolutional model generates the rock failure time in real time based on the input DCC evolution curve.

5.2. Real-time prediction of rock failure time

Fig. 12 presents the real-time prediction results of the failure time for different rocks. The horizontal axis represents the time at which the failure time is predicted, the vertical axis denotes the corresponding predicted rock failure time, and the red dotted line indicates the actual rock failure time. As illustrated in Fig. 12a, the actual failure time of marble1 is 826 s, while the convolutional model predicts the rock failure time to be 880 s at 795 s, resulting in a deviation of 55 s from the actual failure time, with the prediction being 86 s earlier than the actual failure time. As the loading process of marble 1 progresses, the error in the predicted failure time gradually decreases, reaching 13 s at 825 s. In Fig. 12b, the actual failure time of granite1 is 764 s. The prediction error gradually decreases during the loading process, with an accurate failure time predicted at 743 s. Subsequently, the error initially increases and then decreases, leading to another accurate prediction at 756 s. In Fig. 12c, the actual failure time of yellow sandstone 1 is 826 s. The predicted time initially lags behind the actual failure time, but the error gradually decreases as the loading process continues, culminating in an accurate prediction at 797 s.

The predicted failure times for marble 1 and granite 1 generally precede the actual rock failure times, whereas the predicted failure times for yellow sandstone 1 and basalt 1 lag behind the actual rock failure times. However, as the rock loading process progresses, the error in the convolutional model's prediction of rock failure time gradually decreases, converging toward the actual rock failure time.

To quantitatively evaluate the predictive performance of the convolutional model regarding rock failure time, the accuracy between the DCC threshold of 0.78 and the rock failure time is utilized as an evaluation metric, calculated as shown in Eq. (3):

$$Accuracy_t = \frac{\sum_{i=1}^{n}\left(\left(t - \left|t_p^i - t\right|\right)/t\right)}{n} \tag{7}$$

where n is the difference between the moment when the DCC reaches 0.78 and the time when the rock is truly damaged; t is the true time of rock failure; t_p^i is the rock failure time predicted by the convolution model at time $t - n + i$ in the uniaxial compression test.

As illustrated in Fig. 12, the prediction accuracy for marble 1, granite 1, yellow sandstone 1, and basalt 1 is 95.89 %, 99.15 %, 97.02 %, and 97.13 %, respectively. These results demonstrate that the CNN-LSTM-Attention convolutional model, based on the DCC index, is capable of promptly outputting the rock failure time once the DCC exceeds the threshold of 0.78. During the real-time prediction process for four different rocks, the accuracy of rock failure time prediction exceeds 95.89 %, with the highest accuracy reaching 99.15 %.

5.3. Final prediction of rock failure time

In the real-time prediction of rock failure time, it is necessary to determine the prediction time before the rock failure and instability, and the evaluation criteria of the prediction time include the advance prediction time and the exact time of the prediction of instability and failure [2]. Combined with the scoring criteria of rock failure prediction time in comments on the competition of short-impending prediction of rock failure, the prediction error rate of small-scale rock specimens with a loading time of less than 9 % is defined as accurate prediction when the loading time is less than 1000 s. CNN-LSTM-Attention is further trained to predict the final prediction result of rock failure time before rock failure.

Table 5 presents the final failure times of different rocks as predicted by the CNN-LSTM-Attention convolutional model. For different rocks, the convolutional model predicts the final failure time within 20 s after the DCC exceeds the threshold of 0.78, with an error rate of less than 9 %. These results demonstrate that the final predictions generated by the convolutional model effectively forecast the rock failure time.

Considering the feasibility of real-time predictions when the model is deployed on-premises, we ran 100 inference tests on the trained neural network on a local machine (Intel's i7-8565U). As shown in Fig. 13, the average inference time is less than 0.6 ms, which can meet the requirements of real-time prediction of rock failure time. We will carefully consider the feasibility of deploying this model on embedded devices for edge deployment in our future work to achieve on-site deployment of the model.

6. Conclusions

In this study, the DCC index into a convolution model is to identify the stable state of rocks and predict failure time, providing a novel methodological approach for geohazard early warning research, facilitating slope instability monitoring and earthquake precursor

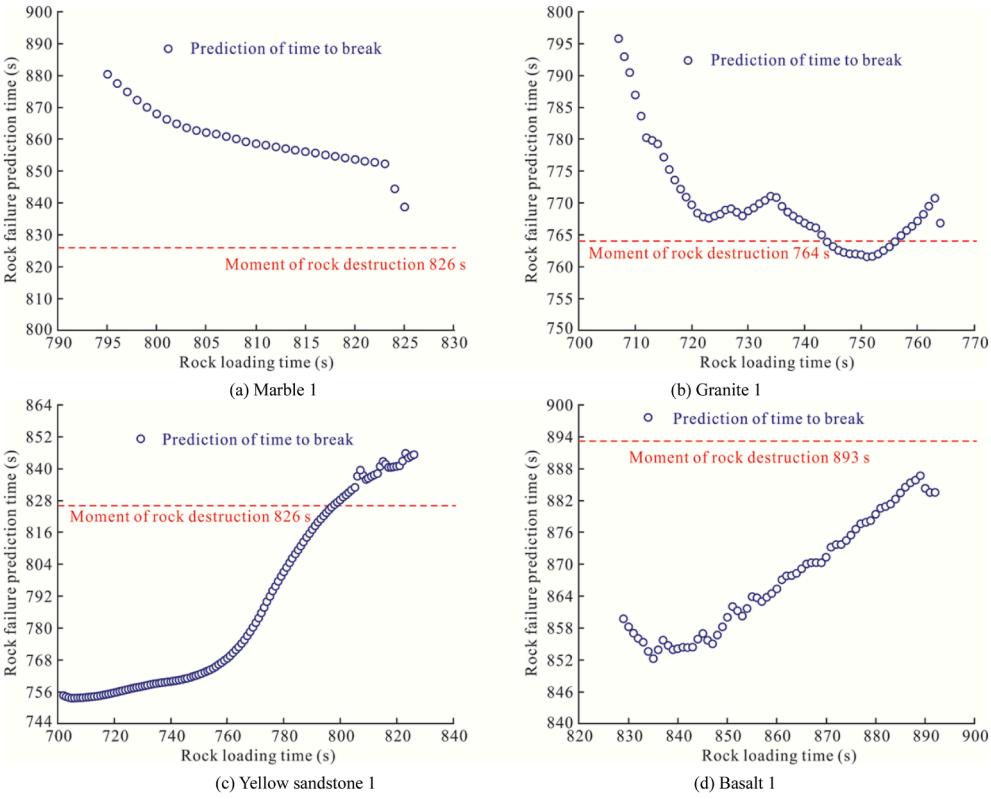

Fig. 12. Prediction results of failure time of different rocks.

Table 5
Final prediction results of the failure time of different rocks.

Rock sample	Rock number	Actual destruction time of the rock (s)	Time when the DCC reached 0.78 (s)	Moment when the convolutional model finally predicts (s)	Convolution models predict rock failure times (s)	Error rate (%)
Marble	DLY-1	826	795	801	866	4.84
	DLY-2	676	649	668	692	2.36
	DLY-3	512	447	458	527	2.92
Granite	HGX-1	764	707	719	771	0.92
	HGX-2	701	637	656	720	2.71
	HGX-3	648	581	596	616	4.93
Yellow sandstone	HSX-1	826	702	722	756	8.47
	HSY-2	670	604	609	692	3.28
	HSY-3	703	644	631	664	5.54
Basalt	XWY-1	893	829	841	854	4.37
	XWY-2	783	714	725	757	3.32
	XWY-3	742	695	610	703	5.26

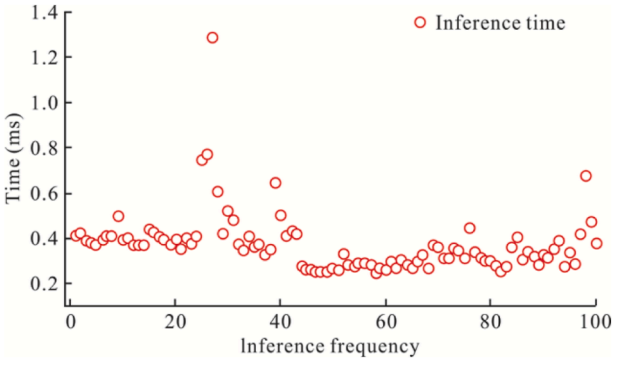

Fig. 13. Inference time.

identification using GNSS and other displacement measurement techniques. The main conclusions are as follows:

(1) The 10 × 10 × 2 data structure demonstrates superior performance compared to the 1000 × 2 × 1 data structure, and the CNN-LSTM-Attention model outperforms the CNN-BiLSTM-Attention and CNN-GRU-Attention models. Under the 10 × 10 × 2 data structure, the CNN-LSTM-Attention model achieves optimal performance in rock stability state identification, with a validation set accuracy of 95.25 % and a recall rate of 96 % for high-risk area samples. By optimizing the data structure of the input variables and the configuration of the convolutional model, the accuracy of the prediction results is significantly enhanced.

(2) Utilizing the DCC index as the input variable within the optimal CNN-LSTM-Attention model, the recall rates for medium- and

high-risk areas on the validation set are 95.8 % and 86.5 %, respectively. These results indicate that the model effectively identifies rock stability states.

(3) The CNN-LSTM-Attention model, based on the DCC index, can predict the final rock failure time in real time once the DCC exceeds the threshold of 0.78. For different rocks, the accuracy of the convolutional model in predicting rock failure time exceeds 95.89 %, with a maximum accuracy of 99.15 %. Furthermore, the model predicts the final rock failure time within 20 s after the DCC reaches 0.78, with an error rate of less than 9 %, demonstrating its effectiveness in accurately forecasting rock failure times.

CRediT authorship contribution statement

Weiyang Li: Writing – review & editing, Writing – original draft, Visualization, Validation, Investigation, Data curation, Conceptualization. **Yongxing Shen:** Writing – review & editing, Writing – original draft, Visualization, Validation, Supervision, Methodology. **Zengchao Feng:** Supervision, Project administration, Investigation. **Xuchen Guo:** Visualization, Investigation.

Declaration of competing interest

Zengchao Feng is an editorial board member for Geohazard Mechanics and was not involved in the editorial review or the decision to publish this article. All other authors declare that there are no competing interests.

Acknowledgements

This work was supported by the National Natural Science Foundation of China (No.52474106).

References

[1] Q. Xu, R.Q. Huang, X.Q. Xiang, Prediction of geological disasters in time and space, J. Mt. Sci. (S1) (2000) 112–117.
[2] Z. Feng, Z.X. Lv, Y.S. Zhao, Research progress on short-impending prediction of rock failure—Comments on the competition of short-impending prediction of rock failure, J. Rock Mech. Geotech. Eng. 41 (12) (2022) 2522–2529.
[3] Y.S. Zhao, Retrospection on the development of rock mass mechanics and the summary of some unsolved centennial problems, J. Rock Mech. Geotech. Eng. 40 (7) (2021) 1297–1336.
[4] S.J. Zhou, Research on Critical power-law Singularity Precursor and Failure Time Prediction, Yanshan University, 2020.
[5] D.Z. Song, Q. Liu, L.M. Qiu, J.G. Zhang, Khan Majid, Y.J. Peng, Y.J. Zhao, M. Wang, M.G. Guo, T.T. Hong, Experimental study on resistivity evolution law and precursory signals in the damage process of gas-bearing coal, Fuel 362 (2024) 130798.
[6] Y.S. Pan, Y.M. Song, C.L. Zhu, H. Ren, H.L. Xu, Localization method of coal rock deformation for rock burst prediction, J. China Coal Soc. 48 (1) (2023) 185–198.
[7] J. Wang, J.W. Gong, Z.Y. Zhao, Position, direction of strain localization of rock-like specimens under uniaxial compression and its application to early-warning, Rock Soil Mech. 39 (S2) (2018) 186–194.
[8] X.B. Wang, W.T. Hou, W. Dong, Evaluation of failure precursors of strain field in uniaxial compressed coal samples based on digital image correlation method, J. Saf. Environ. 18 (4) (2018) 1237–1245.
[9] Y.X. Shen, Z.C. Feng, Study on precursor information of rock instability based on displacement increments measured at multiple points, Nat. Hazards 113 (2022) 1713–1727.
[10] H.M. Cheng, Study on Energy Conversion Mechanism and State Identification During Rock Deformation and Instability, China University of Mining & Technology, Beijing, 2022.
[11] Y.X. Shen, Z.C. Feng, D. Zhou, B.C. Zhang, Different rock failure precursors using displacement coordination coefficient, Environ. Earth Sci. 83 (2024) 490.
[12] A. Arif, C.L. Zhang, M.H. Sajib, M.N. Uddin, M. Habibullah, R.M. Feng, M.J. Feng, M.S. Rahman, Y. Zhang, Rock slope stability prediction: a review of machine learning techniques, Geotech. Geol. Eng. 43 (2025) 124.
[13] F.M. Huang, H.W. Xiong, S.C. Chen, Z.T. Lv, J.S. Huang, Z.L. Chang, F. Catani, Slope stability prediction based on a long short-term memory neural network: comparisons with convolutional neural networks, support vector machines and random forest models, Int. J. Coal Sci. Technol. 10 (2023) 18.
[14] M.S Lin, L.M. Zeng, S Teng, G.F. Chen, B Hu, Prediction of stability of a slope with weak layers using convolutional neural networks, Nat Hazards 120 (2024) 12081–12105.
[15] F. Chen, Z. Liang, A. Cao, ConvLSTM for predicting short-term spatiotemporal distribution of seismic risk induced by large-scale coal mining, Nat. Resour. Res. 32 (2023) 1459–1479.
[16] J.Y. Li, D. Chen, E.Y. Wang, H.Z. Yang, S.L. Zhao, H.S. Jia, Y.W. Sun, Y. Song, X. Y. Fan, Enhanced convolutional neural network-based prediction and source mechanism interpretation of high-energy microseismic events in coal mines, Phys. Fluids 37 (4) (2025) 046606.
[17] Y.X. Zhao, H.Q. Qiao, R.H. Xie, J.H. Guo, Lightweight 3D convolution model for failure prediction based on acoustic emission of coal under uniaxial compression, J. Rock Mech. Geotech. Eng. 41 (8) (2022) 1567–1580.
[18] Dengke Zhang, Yang Han, Chuanle Wang, Lei Gao, Hui Lu, Liang Chen, Erbing Li, Time series prediction of tunnel surrounding rock deformation using CPO-CLA integrated model, J. Rock Mech. Geotech. Eng. 17 (12) (2025) 7915–7930.
[19] Xuejiao Li, Chunyu Liu, Dezhi Zhou, Liang Yu, Xingcai Lu, A unified deep learning model for thermoacoustic instability detection in swirl premixed flames based on spatial-temporal features, Aero. Sci. Technol. 159 (2025) 109994.
[20] Qing Wei, Huijin Zhang, Ju Yang, Bin Niu, Zuxin Xu Pm2, 5 concentration prediction using a whale optimization algorithm based hybrid deep learning model in beijing. China, Environ. Pollut. 371 (2025) 125953.
[21] Seyed Mahdi Miraftabzdeh, Mohammed Ali Khan, Navid Bayati, Dario Zaninelli, Deep learning methods and evaluation of the extensive carbon emission predictive solution for Danish grid, Sustain. Energy Technol. Assessments 75 (2025) 104242.
[22] M.J. Shi, B.H. Yang, R. Chen, D.S. Ye, Logging curve prediction method based on CNN-LSTM-attention, Earth Sci. Inform. 15 (2022) 2119–2131.
[23] L.M. Qiu, J.T. Dang, J.G. Zhang, M. Wang, Q. Liu, L.L. Si, Z.Y. Jiang, M. Khan, Investigating nonlinear resistivity characteristics and mechanisms of coal during various loading stages, J. Appl. Geophys. 238 (2025) 105705.
[24] Y.J. Wei, M.F. Xia, F.J. Ke, X.C. Yin, Y.L. Bai, Evolution-induced catastrophe and its predictability, in: Microscopic and Macroscopic simula-tion: towards Predictive Modelling of the Earthquake Process, Springer, 2000, pp. 1945–1957.
[25] M.F. Xia, Y.J. Wei, F.J. Ke, Y.L. Bai, Critical sensitivity and trans-scale fluctuations in catastrophic rupture. Earthquake Processes: Physical Modelling, Numerical Simulation and Data Analysis Part II, Springer, 2002, pp. 2491–2509.
[26] Y.L. Bai, H.Y. Wang, M.F. Xia, F.J. Ke, Statistical mesomechanics of solid, linking coupled multiple space and time scales, Appl. Mech. Rev. 58 (6) (2005) 372–388.
[27] Y. LeCun, L. Bottou, Y. Bengio, P. Haffner, Gradient-based learning applied to document recognition, Proc. IEEE 86 (11) (1998) 2278–2324.
[28] Y. LeCun, B. Boser, J.S. Denker, D. Henderson, R.E. Howard, W. Hubbard, L. D. Jackel, Backpropagation applied to handwritten zip code recognition, Neural Comput. 11 (4) (1989) 541–551.
[29] S. Hochreiter, J. Schmidhuber, Long short-term memory, Neural Comput. 9 (8) (1997) 1735–1780.
[30] K. Cho, B.V. Merriënboer, C. Gulcehre, D. Bahdanau, F. Bougares, H. Schwenk, Y. Bengio, Learning phrase representations using RNN encoder-decoder for statistical Ma-chine translation, Comput. Sci. (2014) 1724–1734.
[31] V. Mnih, N. Heess, A. Graves, K. Kavukcuoglu, Recurrent models of visual attention, in: Proceedings of the 27th International Conference on Neural Information Processing Systems, 2014, pp. 2204–2212.
[32] R.M. Neal, Markov chain sampling methods for dirichlet process mixture models, J. Comput. Graph Stat. 9 (2) (2000) 249–265.
[33] R.A. Fisher, The use of multiple measurements in taxonomic problems, Ann. Eugen. 7 (2) (1936) 179–188.
[34] Z.C. Feng, Y.X. Shen, Y.S. Zhao, Research on earthquake prediction methodology utilizing the displacement coordination coefficient of rock failure and GNSS, Chin. J. Geophys. 67 (11) (2024) 4204–4219, in Chinese.